

Focused Surface Acoustic Wave induced nano-oscillator based reservoir computing

Md. Fahim F. Chowdhury¹, Walid Al Misba¹, Md Mahadi Rajib¹, Alexander J. Edwards²,
Dhritiman Bhattacharya³, Joseph S. Friedman², Jayasimha Atulasimha^{1*}

¹Department of Mechanical and Nuclear Engineering, Virginia Commonwealth University, Richmond, VA
¹{chowdhurymf, misbawa, rajibmm, *jatulasimha}@vcu.edu

²Department of Electrical and Computer Engineering, The University of Texas at Dallas, Richardson, TX
²{alexander.edwards, joseph.friedman}@utdallas.edu

³Department of Physics, Georgetown University, Washington, DC
³dhritiman.bhattacharya@georgetown.edu

We demonstrate using micromagnetic simulations that a nanomagnet array excited by Surface Acoustic Waves (SAWs) can work as a reservoir that can classify sine and square waves with high accuracy. To evaluate memory effect and computing capability, we study the Short-Term Memory (STM) and Parity Check (PC) capacities respectively. The simulated nanomagnet array has an input nanomagnet that is excited with focused SAW and coupled to several nanomagnets, seven of which serve as output nanomagnets. The SAW has a carrier frequency of 4 GHz whose amplitude is modulated to provide different inputs of sine and square waves of 100 MHz frequency. The responses of the selected output nanomagnets are processed by reading the envelope of their magnetization state, which is used to train the output weights using regression method (e.g. Moore-Penrose pseudoinverse operation). For classification, a random sequence of 100 square and sine wave samples are used, of which 80 % are used for training, and the rest of the samples used for testing. We achieve 100 % training accuracy and 100 % testing accuracy for different combination of nanomagnets as outputs. Further, the STM and PC is calculated to be \sim 5.5 bits and \sim 5.3 bits respectively, which is indicative of the proposed acoustically driven nanomagnet oscillator array being well suited for physical reservoir computing applications. Finally, the ability to use high frequency (4GHz, wavelength \sim 1 micron) SAW makes the device scalable to small dimensions, while the ability to modulate the envelope at lower frequency (100 MHz) adds flexibility to encode different signals beyond the sine and square waves demonstrated here.

Keywords: Reservoir computing (RC), surface acoustic wave (SAW), spintronics.

A Recurrent Neural Network (RNN) is a machine learning algorithm, which uses its internal memory to remember previous inputs and hence process time series data e.g., speech, audio, text, weather, etc. Reservoir Computing (RC) is a computational framework where a fixed, non-linear reservoir maps the inputs into higher-dimensional space and the readout is trained with linear regression and classification¹. A RC network consists of inputs, reservoirs, and outputs (Fig. 1(a)). In a RC network, only the output weights are trained with fast and simple linear regression method (e.g., Moore-Penrose pseudoinverse). Such physical reservoir implementations are suitable for edge devices that could need to learn in real time. An ideal physical reservoir should have short-

term memory effect and non-linear dynamics as well as manufacturability with minimal circuitry. Various Physical RC (PRC) systems are proposed by researchers such as photonic [20-21], electronic [2], spintronic PRC [2-4,6-11], etc. Each of these physical reservoirs has respective advantages and disadvantages.

Spintronic nanomagnetic devices are well suited for physical reservoir computing due to their inherent interactive non-linear dynamics, recurrence characteristics, enduring lifetime, CMOS-compatibility, and low energy consumption²⁻³. Spintronic physical reservoir computing has been simulated or experimentally implemented using dipole-coupled nanomagnets [12], spin-torque nano-oscillators (STNOs)^[11], spin-wave systems [22], and different skyrmion fabrics [4,6-7]. The skyrmion fabrics include the magnetic textures interpolating between single skyrmions, skyrmion lattices and magnetic domain walls⁴⁻⁵. Simple pattern recognition task can be performed with skyrmion fabric reservoir, which utilizes the recursive response of the magnetization dynamics⁶. Complex tasks such as image classification are also performed by a single magnetic skyrmion memristor (MSM) with current pulse stimulation^{4,7}. Several studies have proposed domain wall (DW) based neurons and synapses for CMOS integrated hybrid computing⁸⁻¹⁰. Different machine learning tasks such as sine and square waves classification, spoken digit, hand-written digit, non-temporal data recognition has been performed using the dynamics of individual domain walls in a nanowire¹⁰. Apart from skyrmion textures and domain walls, vortex-type spin torque oscillator¹¹, magnetic-dipole interactions¹² can be used as a resource for nonlinear dynamics of a spintronic reservoir. Higher computational capabilities can be achieved using forced synchronization¹¹, by increasing number of STNOs, or at the boundary between synchronized and disordered states¹³. As a proof of concept of physical neuromorphic computing, spoken digit recognition task is performed by a magnetic tunnel junction (MTJ) with a comparable accuracy to that of a neural network³. While research on physical reservoir implementation is constantly evolving, the search for an ideal reservoir even for specific applications is still an open problem.

Recently, strain-mediated nanomagnet devices were demonstrated for memory applications through resonant surface acoustic wave (r-SAW) assisted spin-transfer-torque [1]. Unlike memory application, reservoir computing does not require the nanomagnets to switch to an orthogonal state or undergo complete reversal. Hence, the energy barrier ($E_b = K_u V \sim 1\text{eV}$) constraint, associated with volume (V), and perpendicular anisotropy constant (K_u) are not critical to its working. The time-varying SAW induced stress can create ferromagnetic resonance with suitable frequency, which leads to large amplitude precession while being energy efficient. [1]. These advantages motivated us to propose SAW induced magnetization dynamics as an input to nanomagnetic reservoirs. SAWs are generated by interdigitated transducer (IDT) patterned on a piezoelectric substrate which produces Raleigh (transverse) waves. Piezoelectric materials such as Lithium Niobate, can be used to generate such SAW waves that can induce magnetization dynamics in magnetostrictive nanomagnets fabricated on these substrates.

In this work, we demonstrate via micromagnetic simulation that a nanomagnet array, shown in Fig. 1, excited by surface acoustic waves (SAW) can be used as a reservoir to classify sine and square waves with high accuracy. We also evaluate two figures of merit tasks of RC named short-term memory (STM) and parity check (PC) capacity. The STM and PC capacity tasks characterize the memory effect and computing capability of the system, respectively¹⁴. The amplitude of the SAW applied in the input nanomagnet is varied in such a way that its envelope forms random sequence of sine and square waves of 100 MHz frequency. The non-linear responses of the output nanomagnets due to this input are processed by reading the reservoir state in certain intervals and then trained to classify sine and square waves and calculate STM and PC capacity.

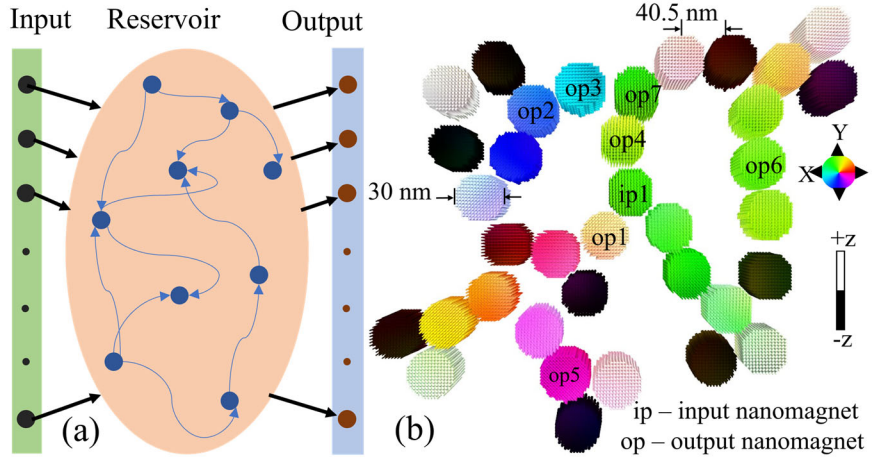


Fig. 1: (a) Concept of reservoir computing (b) A micro-magnetic snapshot of the input, the reservoir and output nanomagnets. The SAW is applied to the input nanomagnet (ip1) and the magnetizations of the output nanomagnets (op1 to op7) are read.

We obtain the free layer magnetization dynamics of the reservoir through micromagnetic simulation with MuMax3¹⁵. The magnetization direction of the reference ferromagnetic layer of an MTJ is fixed and the free layer magnetization is governed by the Landau-Lifshitz-Gilbert (LLG) equation as follows:

$$\frac{d\vec{m}}{dt} = -\frac{1}{(1+\alpha^2)}\gamma[\vec{m} \times \vec{H}_{\text{effective}}] - \frac{\alpha}{(1+\alpha^2)}\gamma[\vec{m} \times (\vec{m} \times \vec{H}_{\text{effective}})] \quad (1)$$

Here, \vec{m} is the normalized magnetization defined as $(\frac{\vec{M}}{M_s})$, \vec{M} is the magnetization, M_s is the saturation magnetization, α is the Gilbert damping coefficient, γ is the gyromagnetic ratio. The effective magnetic field, $\vec{H}_{\text{effective}}$ is comprised of the fields due to shape anisotropy of the nanomagnets, the demagnetizing field, the SAW induced stress, and the exchange field.

$$\vec{H}_{\text{effective}} = \vec{H}_{\text{stress anis}} + \vec{H}_{\text{anisotropy}} + \vec{H}_{\text{demag}} + \vec{H}_{\text{exchange}} \quad (2)$$

$\vec{H}_{anisotropy}$ is the effective field due to shape anisotropy, \vec{H}_{demag} is the field due to demagnetization energy, and $\vec{H}_{exchange}$ is the effective field due to Heisenberg exchange coupling.

The effective field due to the perpendicular magnetic anisotropy, $\vec{H}_{anisotropy}$ is given as:

$$\vec{H}_{anisotropy} = \frac{2K_{u1}}{\mu_0 M_s} (\vec{z} \cdot \vec{m}) \vec{z}. \quad (4)$$

Here K_{u1} is the first order uniaxial anisotropy constant and \vec{z} is the unit vector corresponding to the anisotropy direction.

The effective field due to stress, $\vec{H}_{stress\ anis}$ (in the form of cyclic tension and compression)¹⁶ due to the inverse magnetostriction effect¹⁷ can be expressed as:

$$\vec{H}_{stress\ anis} = \frac{2K_{ut}}{\mu_0 M_s} (\vec{u} \cdot \vec{m}) \vec{u} \quad (3)$$

Here, μ_0 is the magnetic permeability of free space, \vec{u} is the applied stress direction. The stress anisotropy constant, K_{ut} is $\frac{3}{2}\sigma\lambda_s$, where σ is the induced stress by SAW and λ_s is saturation magnetostriction. We consider a uniaxial stress induced by SAW in the \vec{u} direction and neglect the in-plane component which experiences opposite stress (Poisson's effect) orthogonal to \vec{u} . We note that the estimated stress amplitude is conservative due to this assumption, but the qualitative magnetization dynamics remains the same. Since the focused SAW is locally applied in the input region, the induced stress through the piezoelectric substrate in the reservoir or output region is negligible comparatively. So, the stress anisotropy field, $\vec{H}_{stress\ anis} = 0$ and the effective field on the nanomagnets of reservoir or output nanomagnets is comprised of $\vec{H}_{anisotropy}$, \vec{H}_{demag} , and $\vec{H}_{exchange}$.

The schematic diagram of the input, reservoir, and output nanomagnets for the RC simulation is shown in Fig. 1(b). The input nanomagnet is indicated by ip1 and of the rest of the nanomagnets in the reservoir, seven nanomagnets are selected as outputs and denoted by op1 to op7. A 4 GHz focused surface acoustic wave induced stress is applied to the input nanomagnet. We assume the SAW is applied using an interdigitated transducer (IDT) which is patterned on top of a piezoelectric. The simulation dimension is 512 nm x 512 nm x 16 nm that covers all input, reservoir and output nanomagnets, and each cell size is 2 nm x 2 nm x 2.1875 nm, which is much lower than the ferromagnetic exchange length, $\sqrt{2A_{ex}/\mu_0 M_s^2} = 6.32$ nm. The cylindrical nanomagnets are 30 nm in diameter and 35 nm in height. The piezoelectric substrate is assumed to be lithium niobate (LiNbO₃) and the simulation parameters are summarized in table I.

Table I. Simulation parameters for the physical reservoir for the soft ferromagnetic layer of an MTJ

Parameter	Value
Gilbert damping constant, α	0.05
Saturation magnetization, M_s	0.72×10^6 A/m
Exchange stiffness, A_{ex}	13×10^{-12} J/m

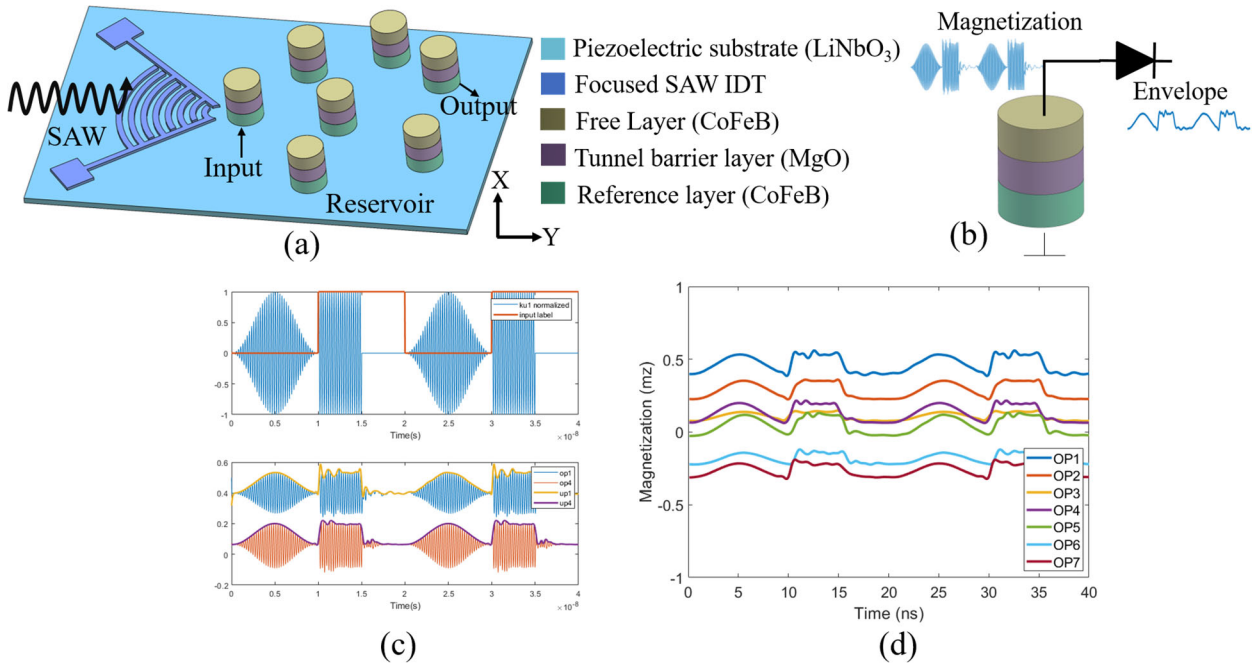


Fig. 2: (a) Application of focused SAW with Inter Digitated Transducer (IDT) chip on the input (b) Reading of magnetization of the output nanomagnet through the soft layer of an MTJ (c) Normalized perpendicular anisotropy applied as SAW and labeling of sine and square waves as 1 and 0 (top), Magnetization output nanomagnets 1 and 4 in response to SAW and their corresponding envelopes (bottom) (d) SAW and input response, the envelopes of the responses vs. time (ns) of several output nanomagnets.

Two fundamental properties required for reservoir computing are: nonlinearity and memory. Due to the nonlinearity and complex dynamics of the reservoir, the network response should be consistent/similar for similar inputs and distinguishable for different inputs. For reservoir computing, we utilize the magnetization dynamics of the input and output nano-oscillators which are governed by the LLG equation described earlier. Further, the input information is encoded in

the envelope of a focused SAW of 4 GHz consisting of a random sequence of sine and square waves, applied to the input nanomagnet as shown in Fig. 2(a). During classification, the sine and square waves are labeled as 1 and 0, respectively. The reservoir computing method [23] is as follows:

$$i_s(n) = \begin{cases} 0, & \text{sine} \\ 1, & \text{square} \end{cases} \quad (5)$$

$$i_s = \{0,1,01, \dots, 1,1,0\}; \quad n \in \{1,2,3 \dots, n_{train}, n_{test}, \dots, n_{max}\} \quad (6)$$

$$s^n = [s_1^n \ s_2^n \ s_3^n \ \dots \ s_N^n] \quad (7)$$

In each period, the non-linear magnetization response (or magnetoresistance due to magnetization orientation of the soft layer of the MTJ) of the reservoir is read N times in an interval τ , where $\tau = \frac{T}{N}$, T = period of sine or square, and N = number of virtual nodes. Here, s^n =virtual node vector and the measured virtual nodes represent the states of the reservoir nanomagnets and form envelopes.

The current state of the reservoir depends on the current input and the previous state of the reservoir, which represents the memory effect of the reservoir.

$$s^n(N+1) = f[s^n(N), i_s(n)] \quad (8)$$

The optimum weights are obtained by linear Moore-Penrose pseudo-inverse operation to the training data. The optimized output weight is called learning and used to predict the output. The mean square error (MSE), the optimized weight matrix (W_{out}) are expressed as:

$$MSE = \frac{1}{n_{train}} \sum_{n=1}^{n_{train}} (y_{train}^n - W_{out}^T s^n)^2 \quad (9)$$

$$W_{out} = y_{train}^t * pinv(s^t) \quad ; \quad t = \{1,2,3 \dots, n_{train}\} \quad (10)$$

Here, $pinv$ finds the Moore-Penrose pseudoinverse of a matrix. Suppose the W_{out} thus evaluated is:

$$W_{out} = [W_1, \ W_2, \ \dots, \ W_N] \quad (11)$$

Then output of the reservoir (denoted as y_{out}) is obtained by the matrix multiplication of the learned weight and reservoir state or test data of the network.

$$y_{out} = W_{out} s^v \quad ; \quad v \in \{n_{test}, \dots, n_{max}\} \quad (12)$$

$$y_{out} = [W_1, W_2, \dots, W_N] \begin{bmatrix} s_1^{n_{test}} & s_1^{n_{test}+1} & \dots & s_1^{n_{max}} \\ s_2^{n_{test}} & s_2^{n_{test}+1} & \dots & s_2^{n_{max}} \\ \vdots & \vdots & \ddots & \vdots \\ s_N^{n_{test}} & s_N^{n_{test}+1} & \dots & s_N^{n_{max}} \end{bmatrix} \quad (13)$$

We evaluate the quantitative performance of the reservoir with Short-Term Memory (STM) task and Parity Check (PC) task [24]. STM task characterizes the memory effect of the system by generating delayed inputs and testing if the internal dynamics of the reservoir is trained to adjust with the delay. The training and testing input data for STM is given below:

$$y_{STM}^{n,d} = i_s(n - d) \quad (14)$$

Here, d = introduced delay. The STM task is not sufficient to prove reservoir property, so the parity check (PC) task is introduced. The PC task characterizes the non-linearity of the system which is indicative of the computing capability of the system and simplifies the training of the reservoir. The training and testing data for PC task is prepared with modulo(2) operation to introduce non-linearity and is expressed as follows:

$$y_{PC}^{n,d} = [i_s(n - d) + i_s(n - d + 1) + \dots + i_s(n)] \bmod(2) \quad (15)$$

Once the learned weights are obtained, the correlation coefficient between testing data, $y_{STM/PC}^{n,d}$ and output data y_{out} are calculated. The total capacities for STM (C_{STM}) and PC (C_{PC}) tasks are calculated by integrating (summing in the discrete case) the correlation coefficients for delay up to d_{max} .

$$r_{STM/PC}(d) = \sqrt{\frac{\text{covariance}[y_{STM/PC}^{n,d}, y_{out}]}{\text{variance}[y_{STM/PC}^{n,d}] \text{variance}[y_{out}]}} \quad (16)$$

$$C_{STM/PC} = \sum_{d=0}^{d_{max}} [r(d)]^2 \quad (17)$$

Fig. 2(a) shows an example of the experimental setup of the proposed reservoir with the application of focused SAW. The focused SAW IDT and the reservoir are fabricated on a piezoelectric substrate, which is assumed to be lithium niobite (LiNbO_3). The input, reservoirs, and outputs are realized by magnetic tunnel junctions (MTJs), made of two CoFeB layers (free layer and reference layer) separated by a tunnel barrier layer (MgO). The free layer magnetization responses are read from the output nanomagnets and preprocessed to obtain envelopes by spline interpolation over local maxima separated by at least 3 samples [25]. The upper envelopes of the output nanomagnets are shown in Fig. 2(d). Each sine or square signal is sampled into N nodes separated by a sampling time τ . The node density can be increased by introducing virtual

nodes^{18,19}. The signals are labeled as 0 and 1 in response to the sine and square waves, respectively. The weights are obtained by linear regression method explained above.

To quantify the performance of the proposed reservoir, the sine and square wave classification is performed by the reservoir as a first task. Although simple, this classification task requires non-linearity and memory effects of the system to predict or classify these waves with high accuracy. The input is a random sequence of 100 sine and square waves with equal period of 10 ns. The first 80 signals are used to train, and the next 20 signals are used to test the reservoir for signal classification, short term memory task, and parity check tasks. The reservoir is able to achieve 100 % training and 100 % testing accuracy with any of the output nanomagnets. The training and testing are performed for different number of virtual nodes 5, 10, 20, 25 and 50. And 100 % recognition rate in both training and testing was achieved for all these number of nodes.

To further evaluate the performance of the reservoir, we studied two fundamental characteristics: fading memory and non-linearity. To evaluate the memory of the proposed reservoir we have calculated STM capacity and to evaluate the nonlinearity, we have performed the PC task and results are discussed next.

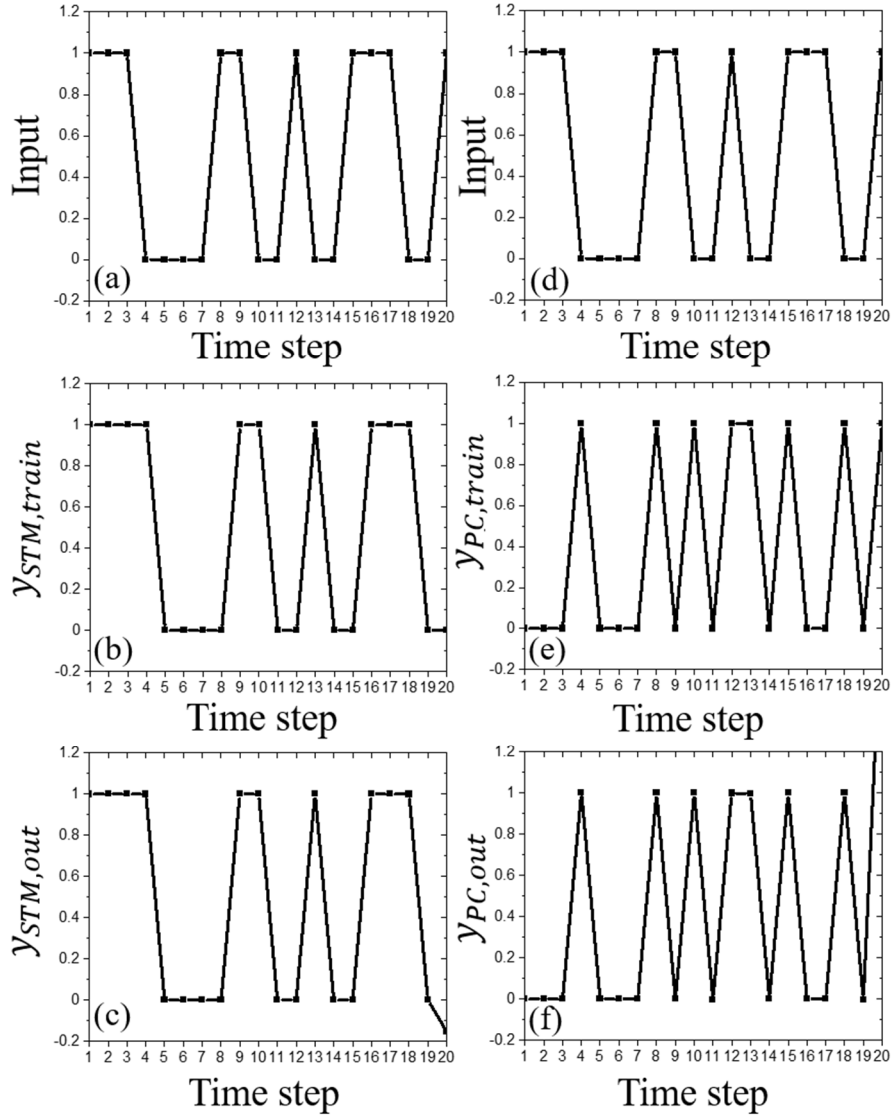


Fig. 3: The SAW input data (i_s) for STM (a) and PC (d) tasks. The training sequence of the input for (b) short-term memory task ($y_{STM,train}$) at delay, $d_{STM} = 1$ and (e) parity check task ($y_{PC,train}$) at $d_{PC} = 1$. The (c) STM output data ($y_{STM,out}$) and PC output data ($y_{PC,out}$). The virtual node number, $N = 20$. The output nanomagnet op_3 .

Typical results for reservoir computing capabilities are demonstrated in Fig. 3, 4, and 5. The input data (i_s), training data for STM ($y_{STM,train}$), and PC ($y_{PC,train}$) tasks, and the corresponding output data ($y_{STM,out}$ and $y_{PC,out}$) are shown in Fig. 3. The training data for the STM (Fig. 3(b)) and PC tasks (Fig. 3(e)) are defined in Eqs. (14) and (15), respectively. The output is calculated using the magnetization dynamics of the output nanomagnet, op_3 and the number of virtual nodes per signal, $N = 20$. The optimized weights, W_{out} are obtained using Eq. (10). The output data fits the training data for both STM and PC tasks at delay, $d_{STM} = 1$ and at delay, $d_{PC} = 2$,

respectively, which corresponds to square of the correlation coefficient, $r^2 = 1.0$ calculated by Eq. (16).

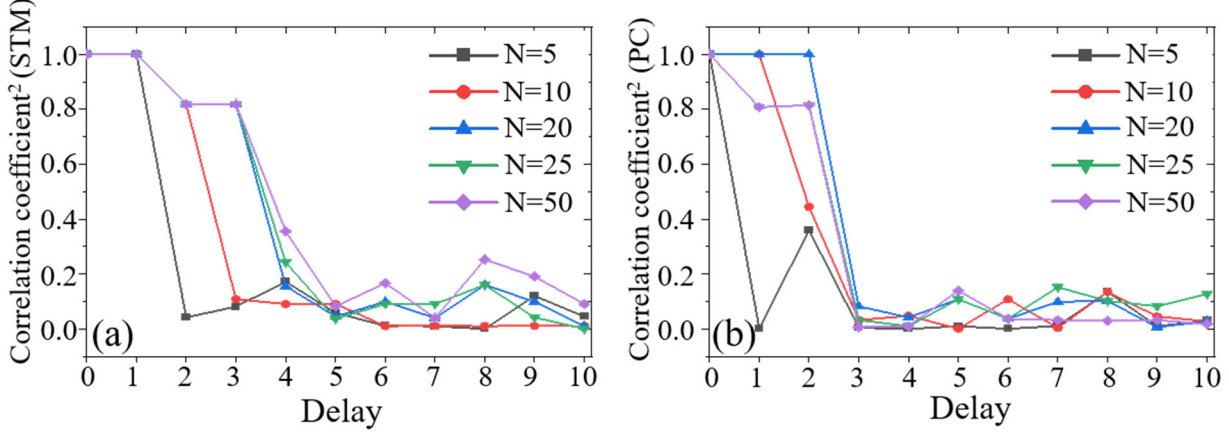


Fig. 4: (a) Square of correlation coefficient, $r_{STM}^2(d)$ for STM task in terms of delay and number of virtual nodes, (b) square of correlation coefficient, $r_{PC}^2(d)$ for PC task in terms of delay and number of virtual nodes.

Fig. 4(a) shows the square of the correlation coefficient, $r_{STM}^2(d)$ between the training data of short-term memory task, $y_{STM}^{n,d}$ and output data, y_{out} as a function of delay from $d = 0$ to $d = 10$. Each of the time step corresponds to 10 ns delay. The STM correlation coefficient², $r_{STM}^2 = 1$ for all the number of virtual nodes, N in consideration at delay, $d = 1$ and starts to decrease with the increase of the delay. The $r_{STM}^2(d)$ tends to be higher in general with the increase in the number of the virtual nodes. Similarly, Fig. 4(b) presents the square of the correlation coefficient, $r_{PC}^2(d)$ between the training data of parity check task, $y_{PC}^{n,d}$ and output data, y_{out} as a function of delay from $d = 0$ to $d = 10$. Similar trends as STM have been observed for the PC task, for the correlation coefficient, as a function of the number of virtual nodes, and delay.

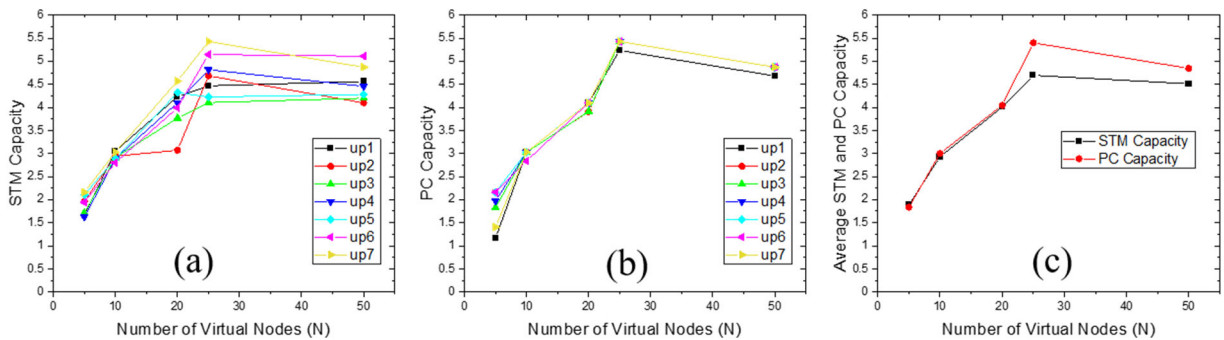


Fig. 5: (a) Short-Term Memory capacity (C_{STM}) and (b) Parity Check capacity (C_{PC}) of the output nanomagnets as a function of the number of virtual nodes (c) Average STM and PC capacity of the output nanomagnets as a function of the number of virtual nodes.

The dependency of Short-Term Memory capacity (C_{STM}) on the number of virtual nodes in each wave (N) is shown in Fig. 5(a). There is a general tendency of increasing STM capacity with increasing number of virtual nodes for all the output nanomagnets. Fig. 5(b) shows the Parity Check capacity (C_{PC}) vs virtual node numbers (N) follows similar characteristics as STM task. The average STM and PC capacity of seven output nanomagnets are shown in Fig. 5(c) in terms of the virtual node numbers. The reservoir has an average STM capacity of ~ 4.5 and PC capacity of ~ 5 bits.

In summary, we have introduced a spintronic physical reservoir where a focused SAW is applied in the input. The non-linear response of the output nanomagnets are processed and output weights are trained through simple linear regression. The reservoir is able to identify sine and square waves with 100 % accuracy. In addition, we have demonstrated the expressivity of the reservoir by evaluating two figures of merit for RC. We have achieved maximum capacities of ~ 5.5 and ~ 5.3 for STM and PC respectively, which are indicative of a viable physical reservoir. Finally, the ability to use high frequency SAW makes the device scalable to small dimensions, while the ability to modulate the envelope at lower frequency (100 MHz) adds flexibility to encode different signals beyond the work in this paper. This could be key to applications such as speech recognition, anomaly detection, etc. using in-situ learning in edge devices.

Acknowledgment: M.F.F.C, W.A.M, M.M.R. and J.A are supported in part by the National Science Foundation grant CCF-1815033.

References

1. Lukoševičius, M. and Jaeger, H., 2009. Reservoir computing approaches to recurrent neural network training. *Computer Science Review*, 3(3), pp.127-149
2. Tanaka, G., Yamane, T., Héroux, J.B., Nakane, R., Kanazawa, N., Takeda, S., Numata, H., Nakano, D. and Hirose, A., 2019. Recent advances in physical reservoir computing: A review. *Neural Networks*, 115, pp.100-123.
3. Torrejon, J., Riou, M., Araujo, F.A., Tsunegi, S., Khalsa, G., Querlioz, D., Bortolotti, P., Cros, V., Yakushiji, K., Fukushima, A. and Kubota, H., 2017. Neuromorphic computing with nanoscale spintronic oscillators. *Nature*, 547(7664), pp.428-431.
4. Bourianoff, G., Pinna, D., Sitte, M., & Everschor-Sitte, K. (2018). Potential implementation of reservoir computing models based on magnetic skyrmions. *Aip Advances*, 8(5), 055602.
5. You, C. Y., & Kim, N. H. (2015). Critical Dzyaloshinskii–Moriya interaction energy density for the skyrmion states formation in ultrathin ferromagnetic layer. *Current Applied Physics*, 15(3), 298-301.

6. Pinna, D., Bourianoff, G., & Everschor-Sitte, K. (2020). Reservoir computing with random skyrmion textures. *Physical Review Applied*, 14(5), 054020.
7. Jiang, W., Chen, L., Zhou, K., Li, L., Fu, Q., Du, Y., & Liu, R. H. (2019). Physical reservoir computing using magnetic skyrmion memristor and spin torque nano-oscillator. *Applied Physics Letters*, 115(19), 192403.
8. Yue, Kun, et al. "A brain-plausible neuromorphic on-the-fly learning system implemented with magnetic domain wall analog memristors." *Science advances* 5.4 (2019): eaau8170.
9. Siddiqui, S. A., Dutta, S., Tang, A., Liu, L., Ross, C. A., & Baldo, M. A. (2019). Magnetic domain wall based synaptic and activation function generator for neuromorphic accelerators. *Nano letters*, 20(2), 1033-1040.
10. Ababei, R.V., Ellis, M.O.A., Vidamour, I.T. et al. Neuromorphic computation with a single magnetic domain wall. *Sci Rep* 11, 15587 (2021). <https://doi.org/10.1038/s41598-021-94975-y>
11. Tsunegi, Sumito, et al. "Physical reservoir computing based on spin torque oscillator with forced synchronization." *Applied Physics Letters* 114.16 (2019): 164101.
12. Nomura, H. (2018). Reservoir computing with dipole coupled nanomagnets array. *ArXiv181013140 Cond-Mat*.
13. Kanao, T., Suto, H., Mizushima, K., Goto, H., Tanamoto, T., & Nagasawa, T. (2019). Reservoir computing on spin-torque oscillator array. *Physical Review Applied*, 12(2), 024052.
14. Furuta, T., Fujii, K., Nakajima, K., Tsunegi, S., Kubota, H., Suzuki, Y., & Miwa, S. (2018). Macromagnetic simulation for reservoir computing utilizing spin dynamics in magnetic tunnel junctions. *Physical Review Applied*, 10(3), 034063.
15. Vansteenkiste, A., Leliaert, J., Dvornik, M., Helsen, M., Garcia-Sanchez, F., & Van Waeyenberge, B. (2014). The design and verification of MuMax3. *AIP advances*, 4(10), 107133.
16. Roe, A., Bhattacharya, D., & Atulasimha, J. (2019). Resonant acoustic wave assisted spin-transfer-torque switching of nanomagnets. *Applied Physics Letters*, 115(11), 112405.
17. Al Misba, W., Rajib, M. M., Bhattacharya, D., & Atulasimha, J. (2020). Acoustic-Wave-Induced Ferromagnetic-Resonance-Assisted Spin-Torque Switching of Perpendicular Magnetic Tunnel Junctions with Anisotropy Variation. *Physical Review Applied*, 14(1), 014088.

18. Appeltant, L., Soriano, M.C., Van der Sande, G., Danckaert, J., Massar, S., Dambre, J., Schrauwen, B., Mirasso, C.R. and Fischer, I., 2011. Information processing using a single dynamical node as complex system. *Nature communications*, 2(1), pp.1-6.
19. Nakajima, Kohei, Helmut Hauser, Tao Li, and Rolf Pfeifer. "Exploiting the dynamics of soft materials for machine learning." *Soft robotics* 5, no. 3 (2018): 339-347.
20. Prucnal, P. R., Shastri, B. J., de Lima, T. F., Nahmias, M. A., & Tait, A. N. (2016). Recent progress in semiconductor excitable lasers for photonic spike processing. *Advances in Optics and Photonics*, 8, 228–299.
21. Ferreira, d. L. T., Shastri, B. J., Tait, A. N., Nahmias, M. A., & Prucnal, P. R. (2017). Progress in neuromorphic photonics. *Nanophotonics*, 6, 577–599.
22. Nakane, R., Tanaka, G. and Hirose, A., 2018. Reservoir computing with spin waves excited in a garnet film. *Ieee Access*, 6, pp.4462-4469.
23. Lukoševičius, M. and Jaeger, H., 2009. Reservoir computing approaches to recurrent neural network training. *Computer Science Review*, 3(3), pp.127-149.
24. Bertschinger, N. and Natschläger, T., 2004. Real-time computation at the edge of chaos in recurrent neural networks. *Neural computation*, 16(7), pp.1413-1436.
25. <https://www.mathworks.com/help/signal/ref/envelope.html#buv7i12-1>